JMEPEG (1996) 5:299-309

Application of a High-Energy-Density Permanent Magnet Material in Underwater Systems

C.P. Cho, C. Egan, and W.P. Krol

This paper addresses the application of high-energy-density permanent magnet (PM) technology to (1) the brushless, axial-field PM motor and (2) the integrated electric motor/pump system for underwater applications. Finite-element analysis and lumped parameter magnetic circuit analysis were used to calculate motor parameters and performance characteristics and to conduct tradeoff studies. Compact, efficient, reliable, and quiet underwater systems are attainable with the development of high-energy-density PM material, power electronic devices, and power integrated-circuit technology.

Keywords
axial field motor, electric motor, FEA modeling, integrated motor/pump, permanent magnet motor

1. Introduction

ELECTRONICALLY commutated, brushless, permanent magnet (PM) motors are emerging as attractive options in undersea vehicle propulsion, industrial drive systems, and linear and rotary actuators as a result of improvements in rare-earth magnet materials, advances in power electronic devices, and availability of power integrated circuits over the last two decades. The gradual improvement in ceramic and other alloys and especially the rapid development of rare-earth magnets, such as samarium-cobalt and neodymium-boron-iron, have provided designers with a significant increase in available energy. These new advanced technologies have made possible the development of a high-power-density, brushless, axial-field, PM motor system that provides a very high torque-to-inertia ratio (Ref 1-3). That PM motor system has in turn led to the development of a novel integrated motor/pump system.

1.1 *Underwater Propulsion Motor Requirements*

With the U.S. Navy's recent focus on brushless, PM electric motor systems technology for long-range underwater propulsion, the design of high-power-density, quiet, and reliable motor systems has become critical in meeting current and future underwater propulsion requirements. Section 2 of this paper describes brushless, PM axial-field motor design that can provide a high-power-density, high-efficiency, and low-noise/vibration propulsion motor utilizing high-energy-density Nd-B-Fe PM material for underwater applications (Fig. 1 and 2).

The overall design process included cogging torque reduction and axial force variation as major design and fabrication issues that were studied using finite-element analysis (FEA) models. The nonlinear behavior of the stator magnetic material, the importance of relative permeability of the PM and stator lamination material, and the complex air-gap geometry dictated using a nonlinear FEA method to obtain an accurate field solution.

Combinations of staggered and unstaggered stators with skewed and unskewed PMs were studied to discover a method to reduce cogging torque. This paper closely examines the effects of stator staggering and presents the tradeoff between cogging torque reduction and axial force variation.

1.2 *Compact Motor/Pump Concept*

The U.S. Navy also needs motor/pump systems that are compact, reliable, and have low noise for its vehicles. Onboard these vehicles, space is severely limited: Pumps are part of auxiliary systems that reduce space otherwise available for payloads. Pumps must have long life and be resistant to shock.

Section 3 of this paper focuses on a novel integrated electric motor/pump system, the concept for which was conceived during the time period of the axial-field design, analysis, and fabrication. This motor/pump system is a combination of a PM axial-field motor and a centrifugal pump, in which the motor

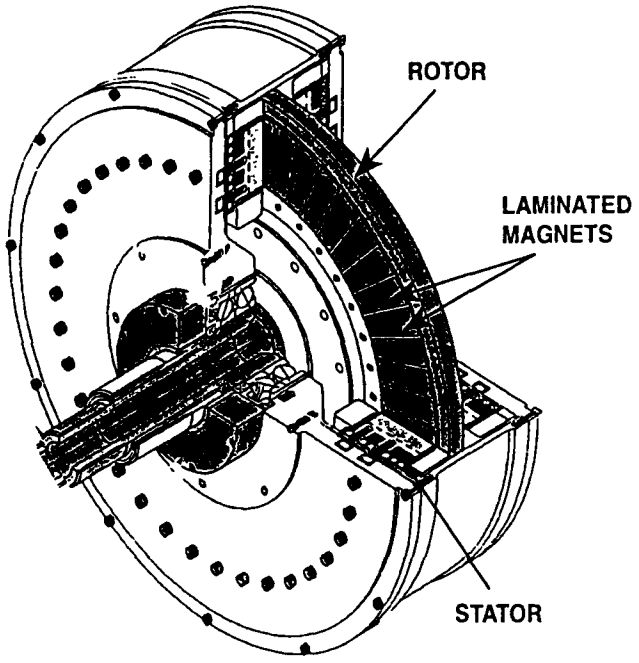

Fig. 1 Cutaway view of a brushless, PM axial-field motor

C.P. Cho, C. Egan, and **W.P. Krol,** Department of the Navy, Naval Undersea Warfare Center Division Newport, Code 8231, Bldg. 1302-2, Newport, RI 02841 USA.

PM rotor and pump impeller vanes are a single part. The purpose of this integrated motor/pump system is to provide a compact, reliable, low-noise, high-power-density, electrically driven centrifugal pump for underwater applications in which minimizing noise, vibration, and volume are major design objectives.

This paper presents the electric motor and pump components, the results of the feasibility study, and manufacturing considerations of the proposed integrated electric motor/pump system. Performance predictions for the electromagnetic design were made using FEA in conjunction with lumped parameter magnetic circuit equations.

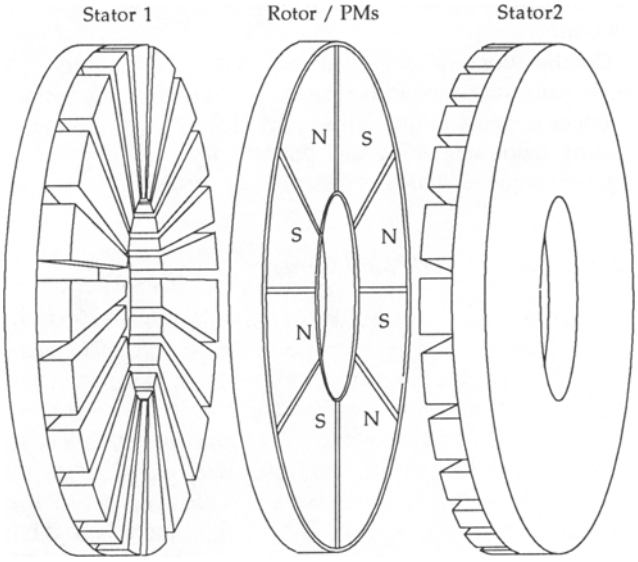

Fig. 2 Simplified axial-field motor

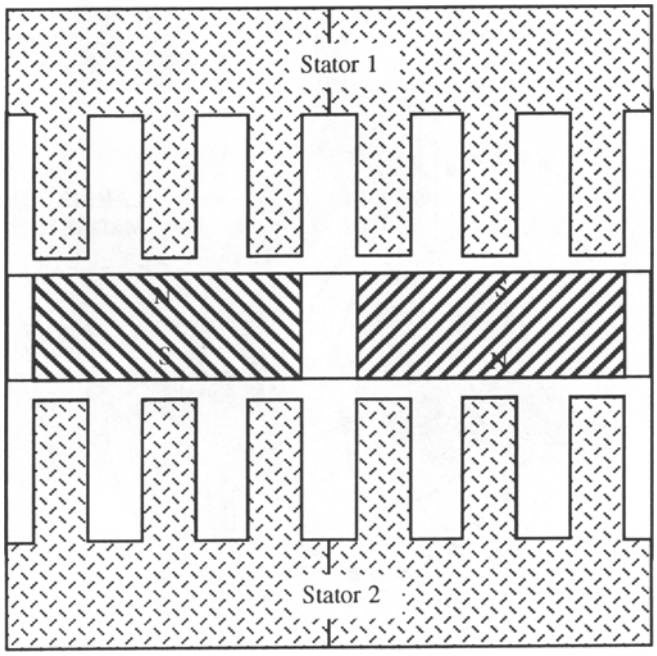

Fig. 3 Two-dimensional one-pole pair section motor model

2. Brushless PM Axial-Field Motor

There are basically three types of axial-field motor configurations: (1) single stator with single rotor, (2) double stator with single rotor, and (3) single stator with double rotor. Figure 2 shows a typical double stator with single rotor axial-field motor configuration. The rotor is a disk structure containing axially magnetized PM blocks. The stator is a disk structure consisting of windings, slots, and teeth. The stator for an axial-field motor configuration is a radial array of current-carrying conductors (motor windings) with appropriate end turns fixed in the stator slots.

The double stator with single rotor configuration has advantages over the other configurations. Precise positioning of the rotor between the two stators produces less axial attractive force on the rotor and stator surface than does the single-stator motor. The power loss is less because the rotor back iron is eliminated, which decreases the amount of magnetic material. Because of these factors, the motor torque and power can be increased while the ratio of weight to horsepower is decreased. Prototyping the double stator with single rotor configuration identified these additional advantages: (1) The air-gap length can be changed by simply adding or subtracting shimming, a

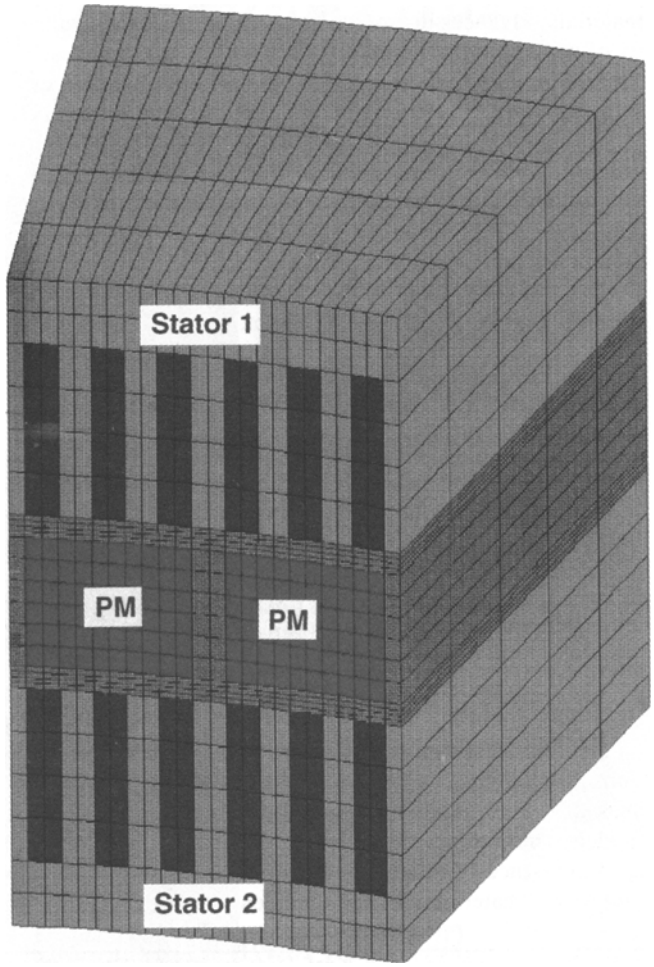

Fig. 4 Three-dimensional one-pole pair section motor model

modification that is not possible in radial-field motor design without refabricating the rotor or stator to change the air gap; and (2) the stator and rotor can be built independently of each other, thus allowing for, in some cases, the rotor diameter to be increased or decreased without rebuilding the stators.

2.1 *FEA Models*

The purpose of using FEA models was to explore the primary flux paths in the electromagnetic system, to check the maximum flux density in the structure for saturation, and to evaluate design and analysis parameters such as back electromotive force (emf) waveform, cogging torque, axial force, and self-inductance. The outlines of the two- and three-dimensional FEA motor models are illustrated in Fig. 3 and 4, respectively.

Figures 3 and 4 demonstrate that motor symmetry of a PM axial-field motor allows a motor to be modeled by a one-pole pair section, or even a one-pole section in some cases, of the full motor. Since most FEA packages are limited in the total number of possible grids, modeling symmetry conditions of the motor permits a finer finite-element mesh and reduced computing time.

2.2 *Axial-Field Motor Tradeoff Study*

In a PM motor, cogging torque is a result of the interaction of the rotor PMs with the teeth and slots on the stator. For a slotted-stator configuration, the air-gap permeance, or reluctance, is nonuniform for three reasons: (1) the shapes of stator teeth and slots, (2) the space between the rotor PM poles, and (3) the saturation of the stator lamination material. These nonuniform reluctances or magnetic flux paths cause air-gap flux density to vary with rotor position and result in cogging torque, which generates noise/vibration when the rotor rotates.

When the PM material energy product is increased rapidly, the reduction of cogging torque becomes a major consideration in the design of PM motors. Cogging torque usually adds an undesirable harmonic component to the torque-angle curve, resulting in torque ripple. Torque ripple produces vibration and noise, both of which may be amplified in variable-speed drives when the torque frequency coincides with a mechanical resonant frequency of the stator or rotor.

At a constant speed, the frequency of the cogging torque is a function of the total number of teeth covered by one rotor PM pole. For example, three teeth covered by one rotor PM pole is one-half of the six teeth covered by the same magnet pole. The magnitude of the cogging force is directly proportional to the air-gap flux or strength of the rotor PM. The cogging torque is not only a function of the total number of teeth covered by the magnet, but is also directly proportional to the ratio of slot to tooth width.

2.1.1 Cogging Torque Reduction Method

This section discusses cogging torque reduction methods and applies those methods to the prototype axial-field motor.

Cogging torque in the axial-field motor configuration can be reduced by (1) skewing of the stator slots or rotor PMs, (2) increasing the number of slots, (3) using semiclosed stator slot openings, (4) using fractional slot/tooth pitch, (5) staggering stators, and (6) reshaping the PMs. Of these six methods, two that have no effect on motor output torque and that can be easily manufactured were selected: rotor PM skewing and stator staggering.

In the first method, skewing of the rotor PMs is accomplished by using specially shaped magnet pieces that have a lopsided appearance (Fig. 5a). The effective cross-sectional area is the same for the unskewed and skewed PMs.

The second method for reducing cogging torque in the double-stator, axial-field configuration is to stagger two stators; that is, one stator is rotated slightly so that its teeth are not aligned with those on the opposite stator (Fig. 5b). Staggering the stators decreases the magnitude of the cogging torque because the air-gap flux changes are less abrupt. A similar phenomenon results from decreasing the slot/tooth pitch and increasing the number of slots and teeth. The frequency is doubled because the total number of slots and teeth exposed to the PM are doubled.

In this study, the cogging (detent) force was calculated as a function of the rotor position using the virtual work method. For each rotor position, a nonlinear, quasi-static field analysis was performed. The cogging forces were then calculated using the virtual work principle method for different rotor positions.

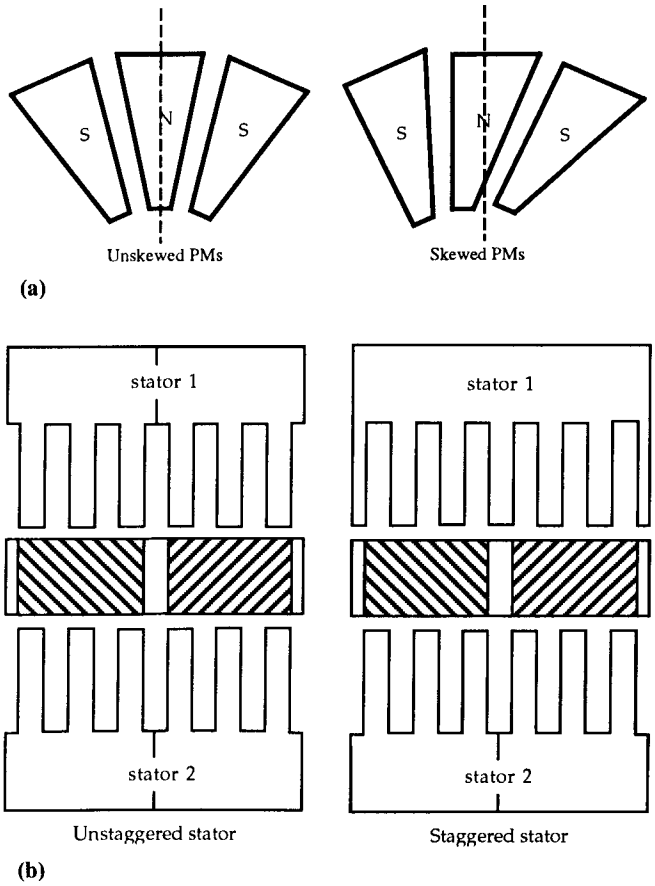

Fig. 5 Cogging torque reduction methods. (a) Skewing permanent magnets. (b) Staggering stators

The virtual work method requires total magnetic coenergy, which can be used to find force using Eq 1. The general expression for force F calculation (Ref 4) is

$$F_x = \frac{\partial W_c}{\partial x} \quad \text{(Eq 1)}$$

where x is any direction, and W_c is the work or magnetic coenergy associated with the force. Equation 2 is derived from the definition of work as force multiplied by distance and is called the virtual work expression for force. An approximated virtual work expression is

$$F_x = \frac{W_c(x + \Delta x) - W_c(x)}{\Delta x} \quad \text{(Eq 2)}$$

where the object on which the force is desired is displaced a small amount, Δx, in the direction of the unknown force.

The cogging torque analysis is sumamrized in Fig. 6, where all possible combinations of the considered cogging torque reduction methods are applied and shown as a function of rotor position in electrical degrees. Experimentally measured peak cogging torque of the prototype motor, with staggered stators and skewed PMs, is also shown in Fig. 6. This measured peak value approximates the peak value predicted by the FEA model.

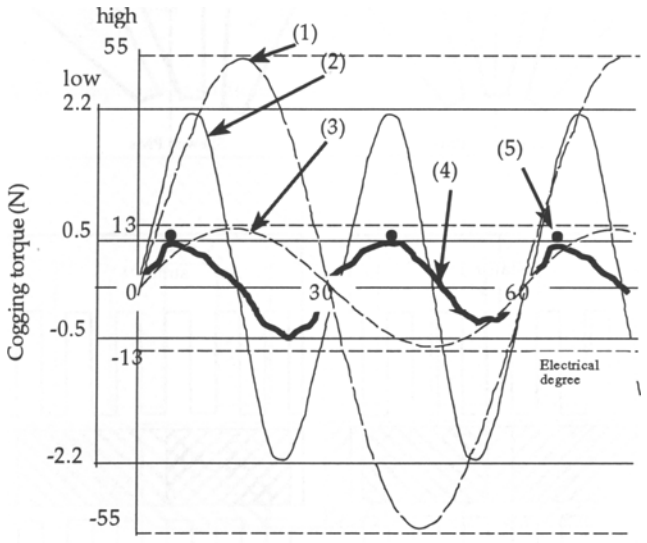

Label	Legend		Scale
1	— —	Unskewed and unstaggered	high
2	———	Unskewed and staggered	low
3	– – – –	Skewed and unstaggered	high
4	▬▬▬	Skewed and staggered	low
5	•	Prototype measured	low

Fig. 6 Graphical summary of cogging torque results

2.2.2 Staggered Stator Effect on Output Torque

As shown, the cogging torque for the staggered stator is reduced to 4% of that for an unstaggered stator. To determine the impact on the output torque by staggering the stators, the torque constant was calculated using the back emf constant. The relationships between the torque constant and the back emf constant are given as:

$$V_{emf} = \omega_m \cdot \frac{d\psi}{d\theta} = \omega_m \cdot K_e \quad \text{(Eq 3)}$$

and

$$T = i \cdot \frac{d\psi}{d\theta} = i \cdot K_T \quad \text{(Eq 4)}$$

where V_{emf} is the generated back emf voltage, ω_m is the rotor revolutions per minute, $d\psi/d\theta$ is the magnetic flux linkage change as a function of the rotor position, K_e is the back emf constant, K_T is the torque constant, and i is the stator phase current in the winding. The torque constant is equal to the back emf constant in the SI system of units.

The back emf constant was calculated using Eq 3 and 4. A wide range of back emf waveforms are measured with motor speed (100 to 1300 rev/min) to calculate the back emf constant. The motor torque constant was calculated from this measured back emf waveform as a function of motor speed.

A test stand consisting of a direct-current (dc) radial field motor as a back-drive motor (Fig. 7) and the axial-field prototype motor was used to measure back emf waveform and vibration measurement. The back emf waveforms were measured using a Tektronix TDS544A (Tektronix, Inc., Beaverton, OR) four-channel digitizing oscilloscope. Because the bed of the test stand was not secured to the ground, the test was conducted between 100 and 1132 rev/min. One stator could be adjusted (depending on the radial staggering angle) and locked in place.

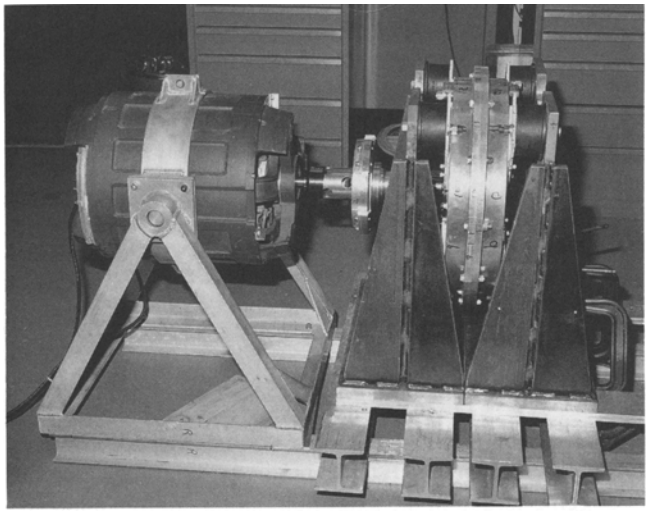

Fig. 7 Back emf and vibration measurement test setup

The staggering angle between two stators was checked by measuring two back emf waveforms of the same-phase terminals from two stators—for example, the back emf waveform 1 from stator 1, phase A, and back emf waveform 2 from stator 2, phase A. By comparing the phase shift of these two waveforms, the accuracy of the stator staggering angle could be measured (Fig. 8).

The back emf waveforms (functions of rotor shaft speed) were measured and plotted. The frequency and peak-to-peak voltage were also recorded in each plot. The back emf constant was calculated by the peak-to-peak emf voltage divided by the rotor speed. Figure 9 shows the back emf peak-to-peak voltage versus rotor speed for the unstaggered and the staggered stator. This plot shows that the two motor torque constants, for unstaggered and staggered stators, are nearly identical. The results indicate that the staggered stator does not affect the output torque, but it does reduce the cogging torque.

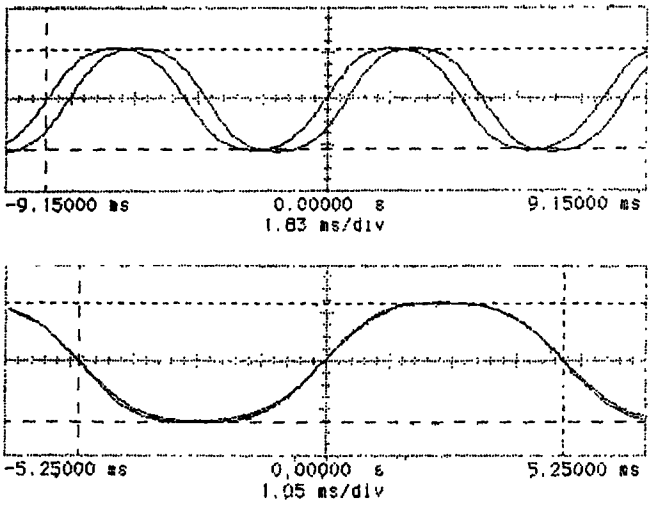

Fig. 8 Staggered and unstaggered stator back emf waveforms

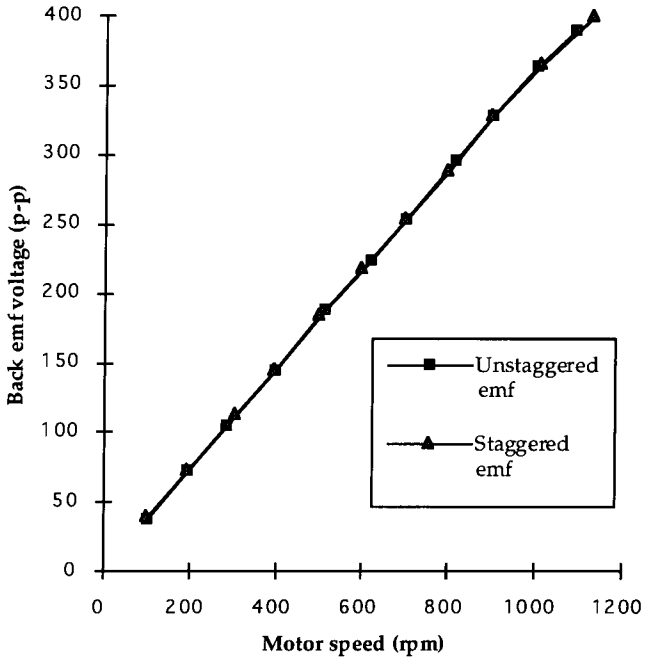

Fig. 9 Comparison of back emf constant

2.2.3 Axial Force Calculation

This section presents the FEA model calculations for the axial force variations on the staggered and unstaggered stator, the consequences of the staggered stator, and the results of a vibration test that was conducted to verify the trends of the axial force variation.

To determine the effect that staggering the stator has on the axial force variation, force calculations for the staggered stator and the unstaggered stator as a function of the rotor position were analyzed using FEA models. Figure 10 shows the axial force results from the unstaggered and staggered stator FEA models.

This result shows that a tradeoff exists between cogging torque reduction and axial force variation and that these factors must be considered in the double-stator, axial-field motor design. Two courses of action could be considered.

The first course of action is a two-step process: (1) build the dual air-gap, axial-field motor with unstaggered stators and skewed rotor PMs, which provides lower axial force variation, and then (2) compensate for the cogging torque by advanced control of the stator currents (Ref 5).

The second course of action is to keep the stator staggered and increase the stator back iron thickness, which reduces the axial force effect. The cogging torque would be minimized and the power density would be reduced by the increased stator back iron thickness (Ref 6).

The results of axial force and cogging torque analyses are provided in Table 1. This table has four major cells of numbers, and each cell is diagonally divided into two triangular subcells. The upper subcell describes cogging torque ratio (based on unstaggered and unskewed), while the lower subcell describes the

Table 1 Cogging torque and axial force tradeoff

Permanent magnets	Unstaggered stators		Staggered stators	
	Cogging torque	Axial force	Cogging torque	Axial force
Unskewed	1	1	1/25	9
Skewed	1/4	1	1/100	9

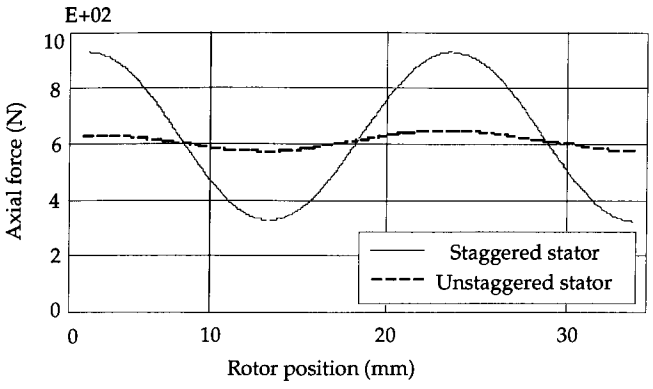

Fig. 10 Axial force variation

axial force ratio. To interpret Table 1, consider the upper left-hand major cell as a baseline, or model, for a motor with unskewed magnets and unstaggered stators. The remaining three major cells contain the factors by which cogging torque or axial force is affected, by either magnet skewing, stator staggering, or a combination of both features. A number less than one means a reduction, whereas a number greater than one denotes an increase.

Although staggering the stators significantly decreases the cogging torque, it increases the axial force variation by a factor of nine. To verify this trend, the axial vibration was measured using an accelerometer attached in the axial direction, while the prototype motor was back-driven by a dc, brushed, radial-field motor. The motor tangential (cogging) and axial vibration were measured for both staggered and unstaggered stator cases, the results of which are shown in Fig. 11(a) and (b). The tangential vibration has been reduced significantly by staggering of stators (Fig. 11a). The experimentally measured axial vibration for the staggered configuration was significantly higher than that for the unstaggered configuration (Fig. 11b). These experimental results are consistent with the results from the FEA models.

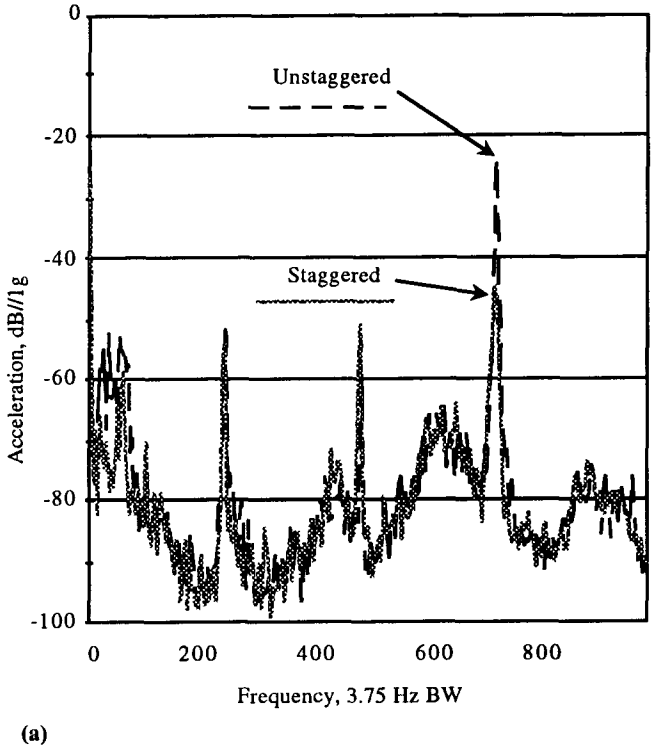

Fig. 11 Vibration test comparison. (a) Tangential vibration. (b) Axial vibration

2.2.4 Summary

Two cogging torque reduction methods (staggering stators and skewing permanent magnets) were studied. Staggered and unstaggered stators with skewed and unskewed permanent magnet combinations were analyzed. By skewing the rotor permanent magnets and staggering the stators, the cogging torque was reduced to 1% of that for a motor with no skewing and staggering, representing a significant reduction. The permanent magnet skewing effect on the cogging torque was analyzed using a developed SIMULAB (The Math Works, Inc., Natick, MA) program.

The most significant factor in reducing cogging torque was stator staggering. However, staggering the stators also increased the axial force variations by almost nine times. The staggered stator effect on output torque was also examined. It was found that staggering the stator has no impact on output torque. In a motor having a light rotor structure, such stresses by axial force variations cause mechanical vibration, noise, and fatigue. A tradeoff between cogging torque reduction and axial force variation was determined. A generic modeling capability program package, with an optimum number of elements and an improved permanent magnet modeling technique (current density method), was used to perform an accurate cogging torque calculation.

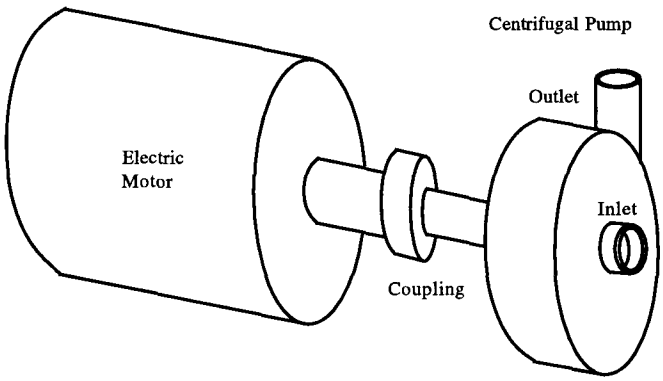

Fig. 12 Traditional electric motor/centrifugal pump set

3. Integrated Motor/Pump Study

A conventionally designed electrically driven centrifugal pump set (Fig. 12) consists of the following components: (1) an electric motor, (2) a coupling system, and (3) a pump. The electric motor torque is transferred through the coupling system (consisting of shafts, bearings, and flexible linkages) to the pump. The pump (encompassing a rotating impeller and stationary casing) transfers energy to the fluid flowing through it, thereby increasing fluid velocity and pressure. The electric current applied to the motor stator also produces waste heat, which must be removed by some means to a lower-temperature heat sink. Machinery arrangements sometimes place severe restrictions on the dimensions of a motor/pump set, especially in the axial direction. Extra space may be required to provide adequate ventilation for cooling or to accommodate a separate cooling system.

Proper alignment between electric motor, coupling system, and pump must be maintained. The coupling system in a traditional motor/pump set compensates for any misalignment between the motor and pump shafts. In many cases, however, this linkage has been identified as a source of undesirable noise and vibration. An integrated brushless, PM axial-field electric motor with a centrifugal pump (Fig. 13) offers advantages over the traditional design. Because the motor and pump in the new design are integral, a separate coupling element is not necessary. Therefore, linkages and bearings, which are primary sources of failure, are eliminated. Additionally, vibration isolation of the motor/pump set from other components is simplified: The PM rotor/pump impeller vibration can be detected using the sensing coils in the motor stator slots, thereby increasing the vibration controllability. Detected behavior of the rotor PM/pump impeller can be used to compensate the vibration using adaptive control or current waveshaping technique.

Because the motor elements of the proposed motor/pump system are in close contact with the fluid being pumped (salt

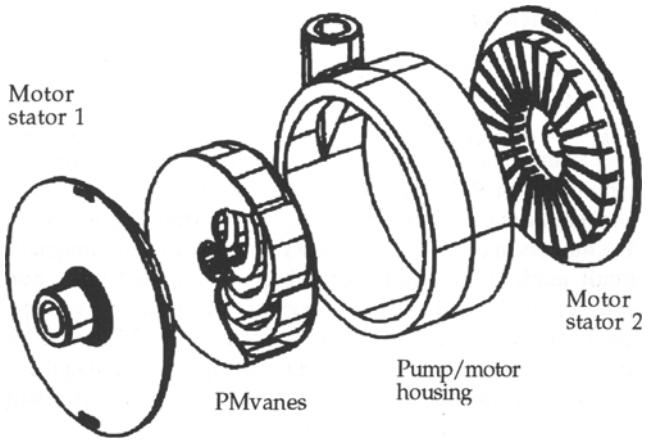

Fig. 13 Exploded view of proposed integrated motor/pump system

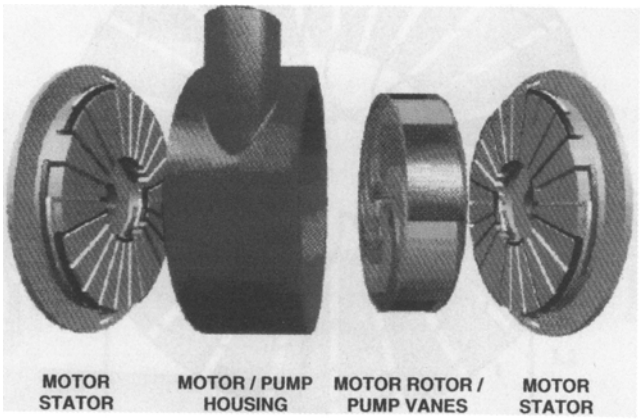

Fig. 14 Exploded view of motor/pump

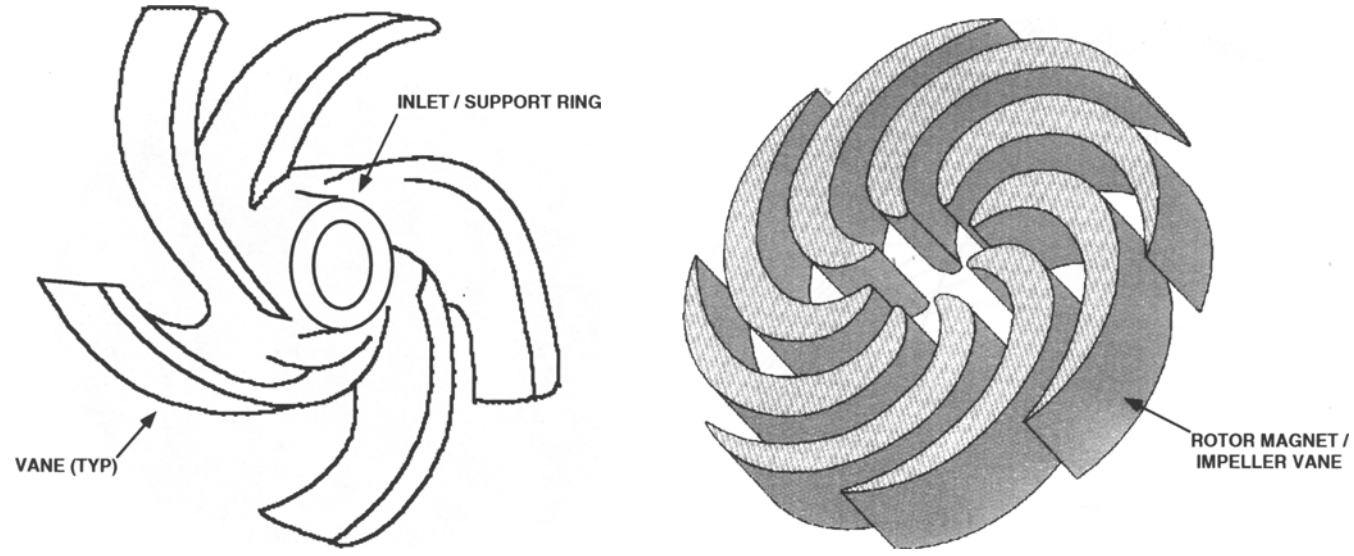

Fig. 15 (a) Typical open impeller. (b) Integrated motor/pump impeller

water in underwater applications), cooling is inherent to the system. Thus, no auxiliary motor cooling system is required.

Furthermore, fewer system components are required for the integrated motor/pump system. Accordingly, production costs are reduced, and potential sources of failure are eliminated while reliability is improved. The required volume, weight, and axial extent of the motor/pump system are reduced, thus freeing up space for payload and allowing greater latitude in the placement of the motor/pump system.

The proposed integrated motor/pump system eliminates the inherent disadvantages of the traditional design. In short, the use of fewer system components reduces production costs, weeds out potential sources of failure, and improves reliability. Figure 14 shows an exploded view of the solid model of the integrated motor/pump system.

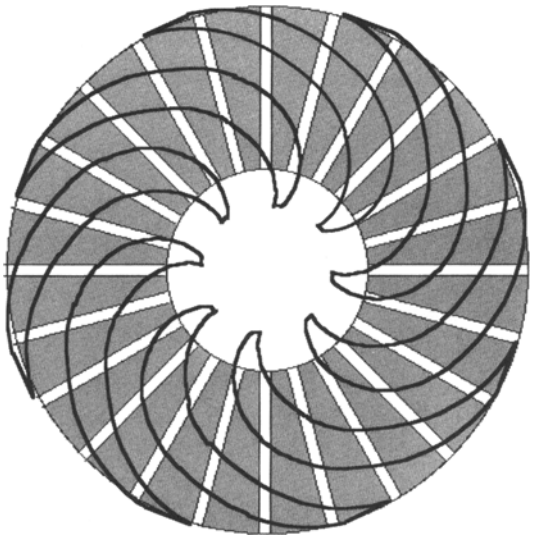

(a)

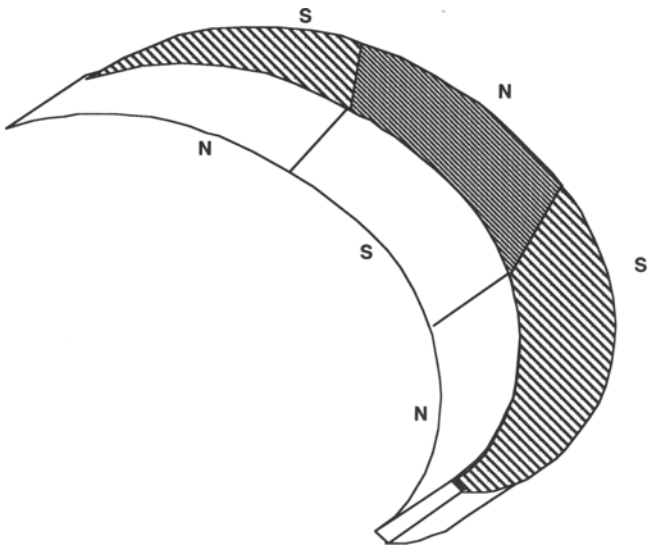

(b)

Fig. 16 (a) Cross section through impeller plane and motor stator. (b) Impeller vane with angular sectors

Figure 15 shows a conventional open impeller and the impeller considered in this study, which is a double-suction, radial-flow, closed impeller. Figure 16(a) is a cross-sectional view through the plane of the impeller and the stator. The impeller consists of a number of vanes attached to two backing plates. (A detailed hydrodynamic analysis is being performed to determine the number and shape of the vanes required to provide a specified capacity and head for a given rotational speed.) The exterior radial region of the vanes corresponding to a similar radial region of the motor stator windings is made of PM material.

Each angular sector of the impeller (Fig. 16b) is assigned a single magnetic polarization. Polarization alternates between adjacent sectors. The number of alternate sectors depends on the number of phases, the number of magnetic poles, and the skewing angle of the impeller vane. The sizing and number of magnetic regions on the impeller are chosen to be compatible with the winding configuration of the motor stators.

3.1 *FEA Models*

Figure 17 shows the FEA model of the rotor/impeller blades used in the research presented in Section 3 of this paper. For the integrated motor/pump study, the stator FEA models are the same as the axial-field motor stator model, the only difference being the rotor PM shape. Performance tradeoffs for the electromagnetic analysis were made by two- and three-dimensional FEA models in conjunction with a lumped parameter magnetic circuit model. The solid computer model served three purposes: (1) It allowed for new concept visualization and animation; (2) it was directly used for electromagnetic FEA analysis for the tradeoff study; and (3) it was also directly translated into a file format for the generation of a physical prototype using stereolithography apparatus (SLA).

3.2 *Tradeoff Study Results*

The electromagnetic tradeoff study used FEA models in conjunction with a brushless, PM axial-field motor lumped pa-

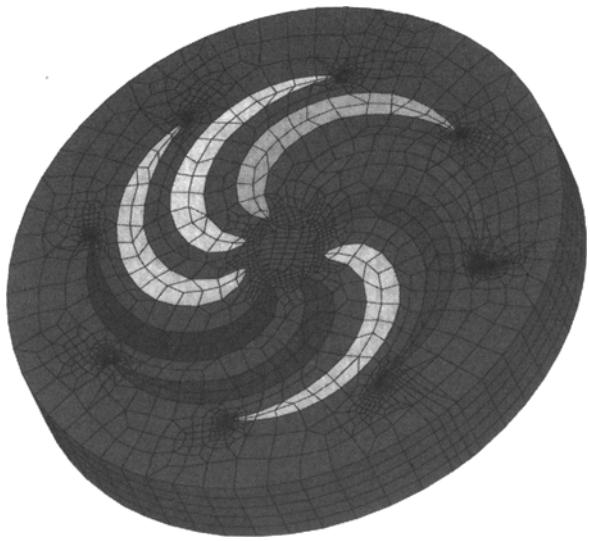

Fig. 17 Three-dimensional FEA model of PM vanes model

rameter magnetic circuit model that was developed using the MathCAD (Math Soft Inc., Cambridge, MA) spreadsheet program. The electromagnetic tradeoff study was based on a 15 hp, 1780 rev/min motor, for which the base specifications included a 250 mm (10 in.) diam, 25 mm (1 in.) rotor axial thickness, 125 mm (5 in.) total axial length, 3-phase, 24-slot, 8-pole, and 2 mm (0.08 in.) air-gap length (Ref 7).

3.2.1 Motor Efficiency, Sectional Area Ratio, and Number of Poles

Figure 18(a) shows the effect on efficiency when varying the sectional area ratio (SAR) between the PM and fluid flow area, but keeping the axial length constant (125 mm, or 5 in.) at 250 mm (10 in.) diameters. Motor efficiency decreases dramatically as the sectional area devoted to PMs decreases.

Figure 18(b) shows the influence that the number of PM poles has on motor efficiency for an SAR of 50%. This result shows that there are an optimum number of PM poles in a given geometry with selected materials.

In Fig. 18(c), the air-gap magnetic flux density in the axial direction, B_y, is calculated for the different SARs. These results allow comparison of the magnetic flux density variation as a function of the SAR. Abrupt changes of the flux density will create large cogging force variation, which is a stray force between the stator and rotor. This result also reveals the tradeoff between the smooth operation versus output torque or power.

In Fig. 18(d), the output power (horsepower) versus motor speed was calculated for varying SAR. The result indicates that at the high-speed operational condition, the eddy current and hysteresis power losses and leakages are the dominant terms so that there is less SAR effect.

3.2.2 Rotor PM/Pump Vane

The shape of the vane changed as the analyses continued. Initially, wedge-shaped vanes were used, but later the vane evolved into a more hydrodynamic form to reflect the actual shape of typical impeller vanes. The rounded inner edge and sharp outer edge caused problems in modeling accuracy until the FEA model was modified to include fine meshes of ele-

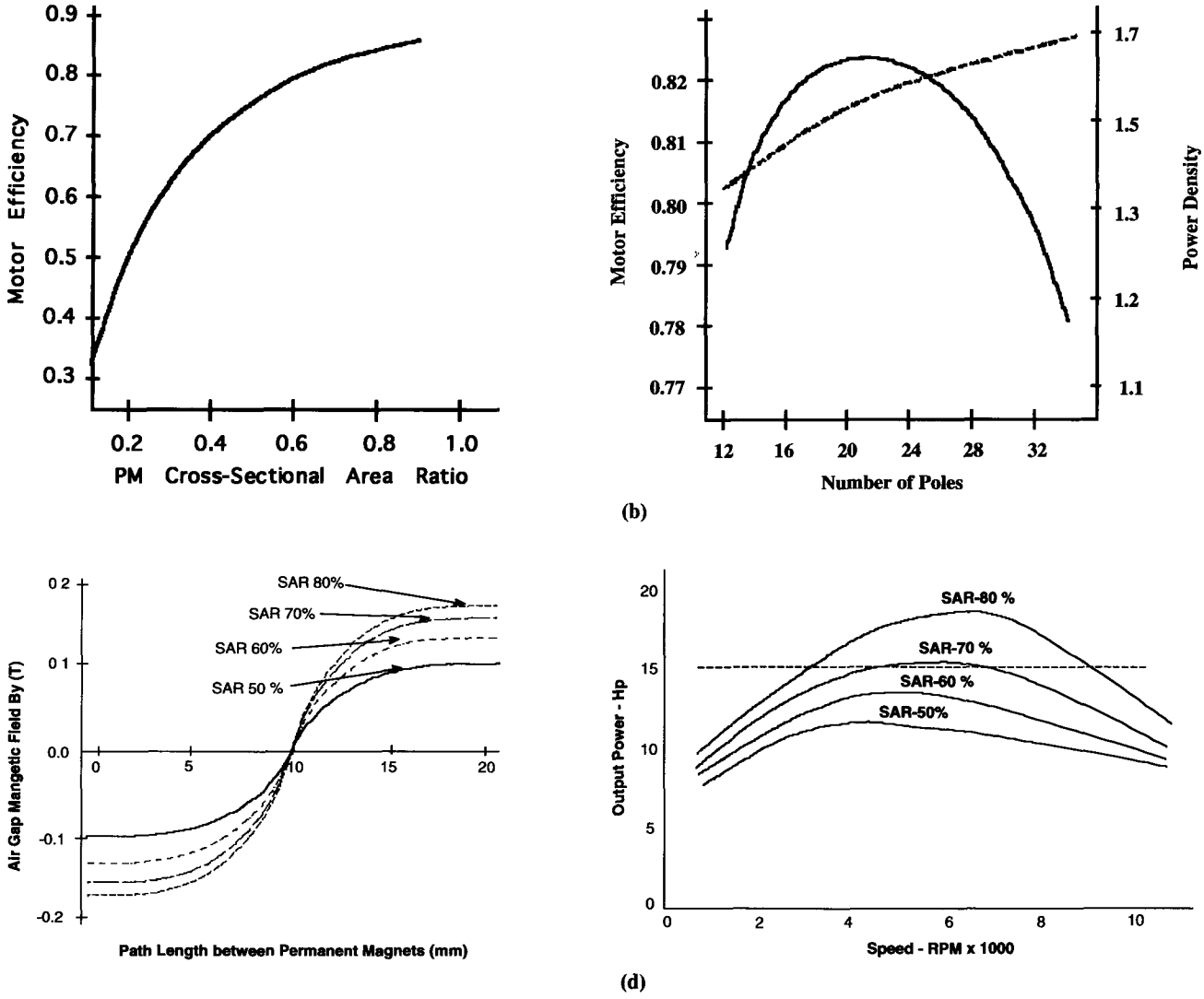

Fig. 18 (a) Motor efficiency versus SAR. (b) Number of poles. SAR = 0.5. (c) Flux density versus SAR. (d) Power versus speed

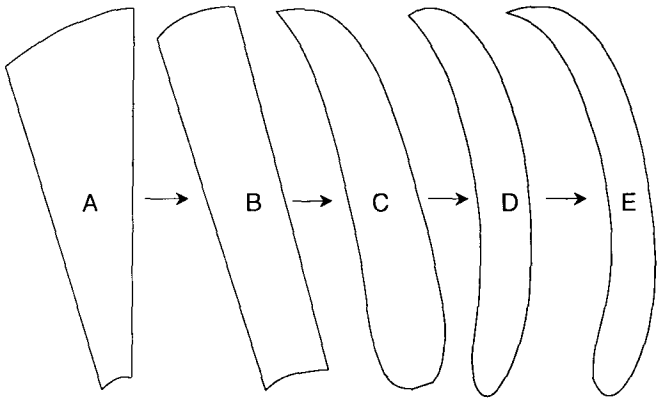

Fig. 19 Rotor/PM vane evolution

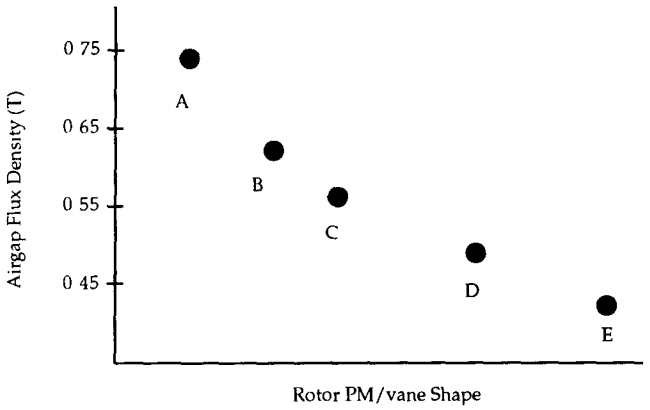

Fig. 20 Rotor/PM vane shape versus flux density

ments in both these areas (Fig. 17). Figure 19 shows the rotor PM vane evolution during the electromagnetic tradeoff study using FEA, and Fig. 20 presents the results. A full analysis must be performed to determine the most efficient vane shape from the standpoint of hydrodynamics.

3.2.3 Manufacturing and Material Selection

Available magnet materials for good motor electromagnetic performance have serious drawbacks as materials of construction for impeller vanes. Constructing useful and efficient impellers offers challenges. For example, the working fluid, salt water, is corrosive to many materials, and some candidate magnets are very chemically active. The vanes must be strong enough to withstand the fluid dynamic forces and centrifugal force as well as the magnetic forces of the motor.

Some candidate magnets, however, are brittle, and some are mechanically weak. Furthermore, optimal magnetic performance dictates the magnetic gap (magnetic flux path through nonpermeable materials and salt water, or air) be as short as possible. Any structural element (such as a stress-bearing plate) between the magnet and the stator increases the gap. In addition, if the plate is an electrically conductive material, eddy currents that diminish performance may be set up by the changing magnetic fields.

Several impeller design options seem plausible. If stresses in the impeller can be kept low, a plastic impeller, such as carbon-fiber-filled polyphenylene sulfide, may be possible. The plastic could be injection molded around the magnets to form a single, chemically sealed unit and serve as the impeller bearing. Another option is that of hollow vanes welded (possibly by electron beam) between two end plates. Magnet sections, previously coated for corrosion protection, are bonded in the interior of the vanes.

3.3 *Rapid Prototyping Using Stereolithography Apparatus*

Stereolithography apparatus, a powerful approach to computer-aided manufacturing (CAM), has ushered in state-of-the-art rapid prototyping and allows important new concepts to be clearly visualized and realized. A solid model of the integrated motor/pump was generated using I-DEAS (Structural Dynamics Research Corporation, Milford, OH) Master Series software. The computer model served three purposes: (1) It allowed concept visualization and animation; (2) it was directly used for FEA using the ANSYS (Swanson Analysis Systems, Inc., Houston, PA) magnetic solver; and (3) it was also directly translated into an STL file format for the generation of a physical prototype. (The SLA used in this study is available at Naval Undersea Warfare Center Division Newport, Code 40, Engineering and Technical Services Department.) The prototype was produced with the SLA-500 machine using a scanned laser beam to harden a photosensitive liquid, Cibatool (Ciba-Geigy Corporation, Los Angeles, CA) SL-5154 acrylate, resin. Newer epoxy-based resins (Cibatool SL-5180) are now available to provide increased accuracy and strength.

Solid computer-aided design (CAD) models are directly used by the system to generate the laser control paths. The rapid prototyping capabilities provide the research and development community with a cost-effective means of going from the conceptual stage to the final product. This method of development was a great demonstration tool that helped convey the new concept to other engineers.

4. Conclusions

This paper analyzed the cogging torque, the axial force variation, and the rotor misalignment effect of a high-horsepower, brushless, dual air-gap, axial-field PM motor. As part of the overall design process, cogging torque, axial force, and rotor misalignment effects were considered as major design and fabrication issues and were studied using quasi-static nonlinear FEA models.

Two cogging torque reduction methods, staggering stators and skewing PMs, were studied. Staggered and unstaggered stators with skewed and unskewed PM combinations were analyzed for methods to reduce cogging torque. A tradeoff between cogging torque reduction and axial force variation was determined. The FEA results were validated by comparing them to experimental measurements obtained from the prototype motor.

The effect of PM skewing on the cogging torque was analyzed using cogging torque analysis in conjunction with a developed SIMULAB program. By skewing the rotor PMs and staggering the stators, the cogging torque was ideally reduced to 1% of that for a motor with no skewing and staggering. The

most significant factor in reducing cogging torque was stator staggering. However, staggering the stators also increased the axial force variations. The effect of the staggered-stator configuration on output torque was also examined. It was found that staggering the stators has no impact on output torque. Stresses by axial force variations cause mechanical vibration, noise, and fatigue in a motor having a light rotor structure.

This paper also presented a novel electric motor/pump system that combines a PM axial-field motor with a centrifugal pump. Based on a tradeoff study, the authors have shown the theoretical feasibility of a new, electric motor/pump concept tailored to meet rigid design criteria for underwater systems. This novel integrated motor/pump has immediate application to the problems faced by designers of underwater vehicle systems. By combining design elements with common functions, using newly available high-technology materials, and operating with a sophisticated control system, severe volume, efficiency, and noise goals can be achieved. The tradeoffs were conducted using three-dimensional FEA models in conjunction with a lumped parameter magnetic circuit model. The results show that this new concept will provide sufficient motor efficiency (up to 73% with 50% SAR) with a given geometry. More research to determine the exact vane geometry for high-hydrodynamic and overall system efficiencies is planned.

Acknowledgments

The research and development described in Section 2 of this paper was sponsored by the Office of Naval Research Exploratory Development Propulsion Program (6.2) Project 01467, Dr. R. Nowak, Program Manager; and Naval Undersea Warfare Center's (NUWC's) New Professional Bid and Proposal (B&P) Program, 1991-1992, as Project 791P54 and 791L37, entitled "High-Power Density Motor Development."

The research described in Section 3 of this paper was sponsored by the NUWC Independent Research (IR) Program as Project B10303, entitled "Novel Integrated Electric Motor/Pump System." The IR program is funded by the Office of Naval Research; the NUWC program manager is Dr. S.C. Dickinson (Code 102). The integrated motor/pump system concept described in this paper has been filed with the U.S. Patent Office through the NUWC Office of Council (U.S. Navy Case No. 76609).

References

1. C.P. Cho and B.K. Fussell, Analysis of a Large-Horsepower Disc Rotor Axial Field, Brushless, Permanent Magnet Motor Using Finite Element and Lumped Parameter Circuit Analysis, *Incremental Motion Control Systems and Devices Proc.*, Incremental Motion Control Systems Society, June 1992, p 105-112
2. G. Amaratunga, P. Acarnley, and P. McLaren, Optimum Magnetic Circuit Configurations for Permanent Magnet Aerospace Generators, *IEEE Trans. Aerosp. Electron. Sys.*, Vol AES-21 (No. 2), 1985, p 2901-2903
3. A.R. Milner, Multi-Hundred Horsepower Permanent Magnet Brushless Disc Motors, *Proc. APEC '94 Conf.*, IEEE Industrial Application, 1994
4. H. Woodson and H. Melcher, *Electromechanical Dynamics, Part II: Fields, Forces, and Motion*, Robert E. Krieger Publishing, 1985
5. J.Y. Hung and Z. Ding, Design of Currents to Reduce Torque Ripple in Brushless DC Motors, *IEEE Proc. B Elec. Power Appl.*, Vol 140 (No. 4), July 1993, p 260-266
6. N.L. Kopp and G.W. Brown, Electric Motor/Controller Design Tradeoffs for Noise, Weight, and Efficiency, *Proc. 1994 Symp. Autonomous Underwater Vehicle Technology* (Cambridge, MA), IEEE and co-sponsored by the Office of Naval Research, July 1994, p 187-193
7. D.M. McGee, "Experimental Studies of Fluid-Borne Noise Generation in a Marine Pump," M.S. thesis, Massachusetts Institute of Technology, May 1993